Organic Electronics 14 (2013) 875–881

Contents lists available at SciVerse ScienceDirect

Organic Electronics

journal homepage: www.elsevier.com/locate/orgel

A star-shaped oligothiophene with triphenylamine as core and octyl cyanoacetate as end groups for solution-processed organic solar cells

Suling Shen [a,b], Lei Gao [b,c], Chang He [b,*], Zhanjun Zhang [a,*], Qingjiang Sun [c], Yongfang Li [b,*]

[a] University of Chinese Academy of Sciences, Beijing 100049, China
[b] Beijing National Laboratory for Molecular Sciences, Institute of Chemistry, Chinese Academy of Sciences, Beijing 100190, China
[c] School of Biological Science & Medical Engineering, Southeast University, Nanjing 210096, Jiangsu, China

ARTICLE INFO

Article history:
Received 23 October 2012
Received in revised form 4 December 2012
Accepted 8 December 2012
Available online 1 February 2013

Keywords:
Organic solar cells
Conjugated organic molecules
Solution processability
Organic photovoltaic materials

ABSTRACT

A new star-shaped D–π–A molecule with triphenylamine (TPA) as core and donor unit, octyl cyanoacetate (CA) as end group and acceptor unit, and 2,2′-bithiophene vinylene (bTV) as π bridge, S(TPA-bTV-CA) was designed and synthesized for the application as donor materials in solution-processed bulk-heterojunction organic solar cells (OSCs). The compound is soluble in common organic solvents. The thermal, optical and electrochemical properties of the star molecule were studied. The OSC devices were fabricated by spin-coating the blend solution of the molecule as donor and $PC_{70}BM$ as acceptor (1:3, w/w). The OSC device based on S(TPA-bTV-CA)/$PC_{70}BM$ demonstrated a high open circuit voltage of 0.91 V, a short circuit current density of 4.64 mA/cm^2, a fill factor (FF) of 50%, corresponding to a power conversion efficiency of 2.1%, under the illumination of AM 1.5, 100 mW/cm^2.

1. Introduction

Bulk heterojunction organic solar cells (OSCs) based on solution-processable small molecular donor materials have attracted much attention recently due to the advantages of high purity and definite molecular weight of the organic molecules in comparison with polymers [1–25]. The solution-processible organic small molecule photovoltaic materials mainly include branched oligothiophenes, linear D–A structured molecules and triphenylamine (TPA)-containing molecules [2–10]. Among the soluble organic photovoltaic small molecular materials, the donor–π conjugated bridge–acceptor (D–π–A) structured organic compounds are regarded as one of the most promising molecular materials [7,8,14,15], because of their broad absorption in visible region resulted from the intramolecular charge transfer (ICT) and easy tuned electronic energy levels and band-gaps through adjusting the acceptor, donor, and pi-bridge units [17,18]. Recently, solution processed small molecule donors have made significant progress and the power conversion efficiency (PCE) of the OSCs based on the small molecule donor reached 6–7% [19,24].

TPA-containing organic molecules have attracted special interest [14,15], owing to their good solubility benefitted from the three dimensional propeller structure of TPA, and higher hole mobility. Many D–π–A structured molecules containing TPA as donor unit have been designed and synthesized for the applications as donor materials in the solution-processed OSCs [2–5,14–17]. Dicyanovinyl (DCN) is a well-known acceptor group and used frequently in the TPA-containing organic optoelectronic materials. For example, Roncali et al. synthesized the star-shaped D–π–A molecules with TPA as core and donor unit, DCN as end group and acceptor unit, and thiophene as the π-bridge [2]. Our group has designed and synthesized a series of TPA–π–DCN based molecules which introduced alkyl side

---

[*] Corresponding authors.
E-mail addresses: hechang@iccas.ac.cn (C. He), liyf@iccas.ac.cn (Y. Li).

1566-1199/$ - see front matter © 2013 Elsevier B.V. All rights reserved.
http://dx.doi.org/10.1016/j.orgel.2012.12.030

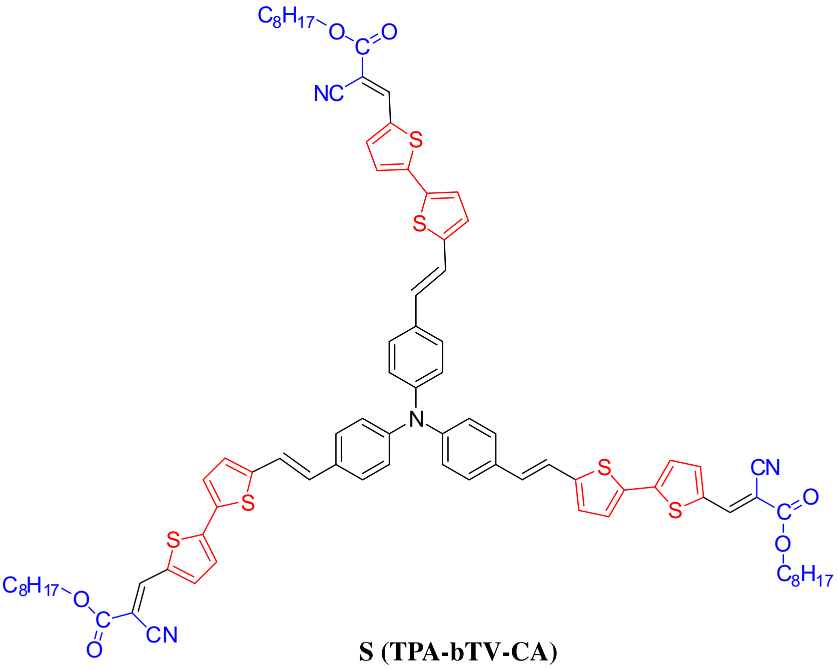

Scheme 1. Molecular structure of S(TPA-bTV-CA).

chains to thiophene bridges [14–17]. These TPA–π–DCN based molecules show good photovoltaic performance, however, the strong polarity of the DCN unit leads to poorer solubility of the molecules [2,16].

Here we designed and synthesized a star-shaped, D–π–A molecule (S(TPA-bTV-CA)) (as shown in Scheme 1) with TPA as core and donor unit, 2,2′-bithiophene vinylene (bTV) as π-bridge, and octyl cyanoacetate (CA) as acceptor unit. The electron withdrawing group octyl cyanoacetate (CA) can improve solubility of the molecules. The compound shows good solubility in common organic solvents as expected, possesses broad and strong visible absorption band, good thermal stability and lower HOMO energy level. In addition, the synthesis process was more time-saving because of the simplified molecular structure. Bulk heterojunction OSCs were fabricated by spin-coating the blend solution of the compound as donor and $PC_{70}BM$ as acceptor. The photovoltaic performance of the OSC device based on a blend of S(TPA-bTV-CA) and $PC_{70}BM$ (1:3, w/w) exhibited a PCE of 2.1% with a short circuit current density (J_{sc}) of 4.64 mA/cm^2, an open circuit voltage (V_{oc}) of 0.91 V, and a fill factor (FF) of 50%, under the illumination of AM.1.5, 100 mW/cm^2. The fill factor (FF) value is among the top values for the OSCs based on the solution-processed TPA-containing organic molecules.

2. Experimental section

2.1. Materials

All reagents were obtained from Aldrich, Acros, or TCI Chemical Co, and were used as received, except that DMF and diethyl ether were freshly distilled prior to use. PCBM was bought from ADS (American Dye Source Inc.) Tetrahydrofuran (THF) was dried over Na/benzophenoneketyl and freshly distilled prior to use. $CHCl_3$ and triethylamine were dried over a molecular sieve. The synthesis routes of S(TPA-bTV-CA) are shown in Scheme 2.

2.2. Measurements and instruments

Nuclear magnetic resonance (NMR) spectra were taken on a Bruker DMX-400 spectrometer. MALDI-TOF spectra were recorded on a Bruker BIFLEXIII. Absorption spectra were taken on a Hitachi U-3010 UV–vis spectrophotometer. The film on quartz used for UV measurements was prepared by spin-coating with 1% S(TPA-bTV-CA) chloroform solution. The TGA measurement was performed on a Perkin–Elmer TGA-7 apparatus. The electrochemical cyclic voltammograms were obtained using a Zahner IM6e electrochemical workstation in a 0.1 mol/L tetrabutylammonium hexafluorophosphate (Bu_4NPF_6) acetonitrile solution. A Pt electrode coated with the sample film was used as the working electrode; a Pt wire and Ag/AgCl were used as the counter and reference electrodes respectively.

2.3. Fabrication and characterization of organic solar cells

Organic solar cells (OSCs) were fabricated in the configuration of the traditional sandwich structure with an ITO positive electrode and a metal negative electrode. Patterned ITO glass with a sheet resistance of 20 Ω sq^{-1} was purchased from CSG Holding Co., Ltd. (China). The ITO glass was cleaned in an ultrasonic bath of acetone and isopropanol, and treated by UVO (ultraviolet ozone cleaner, Jelight

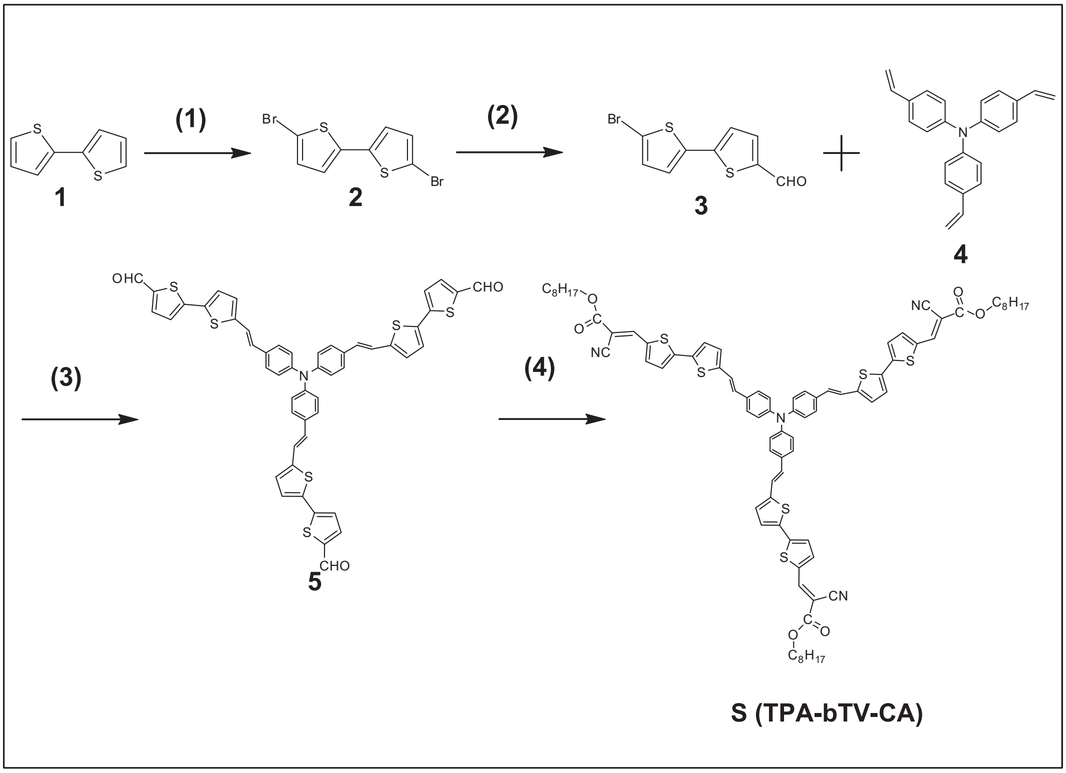

Scheme 2. Synthetic route of S(TPA-bTV-DCA). (1) NBS, DMF, room temperature over night; (2) n-BuLi, THF, DMF, −78 °C; (3) $Pd(OA_C)_2$, $NaOA_C$, n-BuNBr, DMF, 115 °C for 2 days; (4) octyl cyanoacetate, $CHCl_3$, under N_2, triethylamine, 75 °C reflux for 24 h.

Company, USA). Then a thin layer (30 nm) of PEDOT:PSS(poly(3,4-ethylenedioxythiophene):poly(styrene sulfonate)) (Baytron PVP AI 4083, Germany) was spin-coated on the ITO glass. Subsequently, the photosensitive layer was prepared by spin-coating the blend solution of the molecule and PCBM with different weight ratios (1:1, 1:2, or 1:3, w/w) on the top of the PEDOT:PSS layer (over 70 nm thickness). The concentration of the solution was 20 mg/mL in chlorobenzene. The thickness of the photoactive layer was measured using an Ambios Technology XP-2 profilometer. The active layer was thermal-annealed at 80 °C for 10 min, then Ca and Al electrode (ca. 120 nm) was vacuum evaporated, respectively, on the photoactive layer under a shadow mask in the vacuum of ca. 10^{-4} Pa. The active area of the devices is 4 mm^2. The current–voltage (*J*–*V*) measurement of the devices was conducted on a computer controlled Keithley 236 Source Measure Unit. A xenon lamp coupled with A.M. 1.5 solar spectrum filter was used as light source, and the optical power at the sample was 100 mW/cm^2. The input photon to converted current efficiency (IPCE) was measured using a Keithley 2000 System DMM coupled with WDG3 monochromator and 500 W xenon lamp.

2.4. Synthesis

The synthetic route of the compound is shown in Scheme 2. The detailed synthesis processes are as follows.

2.4.1. 5,5′-Dibromo-2,2′-bithiophene **(2)** [17b]

N-Bromosuccinimide (NBS) (11.65 g, 65.450 mmol) was added in small portions to a solution of 2,2′-bithiophene **1** (5 g, 29.76 mmol) in DMF at 0 °C. After being stirred over night at room temperature, the reaction mixture was poured into water (200 mL) and extracted with CH_2Cl_2. The organic layer was thoroughly washed with water, aqueous sodium bicarbonate, brine and again with water, and then dried over Na_2SO_4. After removal of solvent, it was purified by column chromatography on silica gel using petroleum ether as eluant to afford 5,5′-dibromo-2,2′-bithiophene **(2)** (8.20 g, 85%) as a white crystal solid. GC/MS: 324(M^+). ^1H NMR (400 MHz, $CDCl_3$): δ(ppm) 6.97–6.96 (d, *J* = 4.0 Hz, 2H), 6.86–6.85 (d, *J* = 4.0 Hz, 2H).

2.4.2. 5′-Bromo-[2,2′-bithiophene]-5-carbaldehyde **(3)** [18b]

Compound **2** (5.0 g, 15.43 mmol) was dissolved in 200 ml THF in a well-dried flask under the protection of N_2 flow. *n*-BuLi (6.8 ml, 16.98 mmol, 2.5 M in hexane) was added dropwise by syringe under −78 °C. After addition, the reaction mixture was stirred at −78 °C for 2 h and DMF (1.43 ml, 18.52 mmol) was added dropwise, then the mixture was warmed to room temperature. After stirring for 12 h, the mixture was poured into water and extracted with dichloromethane. The organic layer was washed with brine and dried over Na_2SO_4. After solvent removal, the residue was purified by column chromatography on silica gel using petroleum/CH_2Cl_2 5:1 as eluant to afford Compound **3** (2.53 g, 60%) as a yellow solid. GC/MS: 273 (M^+). ^{1}H NMR (400 MHz, $CDCl_3$): δ(ppm) 9.87 (s, 1H), 7.67–7.66 (d, *J* = 4.0 Hz, 1H), 7.19–7.18 (d, *J* = 3.8 Hz, 1H), 7.11–7.10 (d, *J* = 3.8 Hz, 1H), 7.04–7.03 (d, *J* = 4.0 Hz, 1H).

2.4.3. 5′,5‴,5′′′′′-((1E,1′E,1″E)-(nitrilotris(benzene-4,1-diyl))tris(ethene-2,1-diyl))tris(([2,2′-bithiophene]-5-carbaldehyde)) ***(5)***

A mixture of Compound **4** (896 mg, 2.78 mmol), $Pd(OAc)_2$ (37.3 mg, 0.166 mmol), NaOAc (6.82 g, 83.2 mmol), Compound **3** (2.5 g, 9.16 mmol) and *n*-Bu_4NBr (428.7 mg, 1.33 mmol) was dissolved in degassed DMF (40 mL). The solution was kept under a nitrogen atmosphere at 115 °C for 2 days. The mixture was poured into water. The precipitate was filtered, washed with water and dissolved in dichloromethane, and dried over Na_2SO_4. After evaporation of the solvent, the residue was used in the next reaction without any purification.

2.4.4. S(TPA-bTV-CA)

To a solution of residue Compound **5** (0.9 g, 1.00 mmol) in 50 mL of chloroform, octyl cyanoacetate (1.97 g, 10.0 mmol) and 1.5 ml triethylamine were added and the mixture was refluxed at 75 °C for 24 h under nitrogen. After returning to room temperature dichloromethane was added, the solution was washed with water and dried over Na_2SO_4. After solvent removal, the residue was purified by column chromatography on silica gel (petroleum ether:ethyl acetate 1:1) to give 575 mg of black solid with a yield of ca. 40%. MALDI-TOF MS: 1436.3, calculated for $C_{84}H_{84}N_4O_6S_6$ 1436.47. ^{1}H NMR (400 MHz, $CDCl_3$): δ(ppm) 8.25 (s, 3H), 7.67–7.66 (d, *J* = 4.0 Hz, 3H), 7.41–7.38 (d, *J* = 8.0 Hz, 6H), 7.32–7.30 (d, *J* = 8.0 Hz, 3H), 7.25–7.23 (d, *J* = 6.0 Hz, 3H), 7.12–7.08 (d, *J* = 8.6 Hz, 9H), 7.04–7.00 (d, *J* = 10.0 Hz, 3H), 6.96–6.91 (d, *J* = 12.0 Hz, 3H), 4.31–4.27 (t, 6H), 1.79–1.71 (m, 6H), 1.42–1.40 (m, 6H), 1.32–1.29 (d, *J* = 10.0 Hz, 24H), 0.91–0.87 (t, 9H). ^{13}C NMR (400 MHz, $CDCl_3$): δ(ppm) 163.14, 147.55, 146.09, 145.55, 139.24, 134.24, 133.94, 127.70, 127.26, 124.43, 124.24, 116.14, 97.62, 66.65, 31.83, 29.24, 29.21, 22.70, 14.17.

3. Results and discussion

3.1. Synthesis and thermal stability

The synthetic route of S(TPA-bTV-CA) is shown in Scheme 2. Monomer **4** was synthesized according to literature [13]. Compound **5** was synthesized from Monomers **3** and **4** by Heck reaction. The target molecule, S(TPA-bTV-CA), was obtained using a Knoevenagel condensation with yield of 40%. S(TPA-bTV-CA) is soluble in common organic solvents, such as $CHCl_3$, THF, chlorobenzene, and toluene. This solubility satisfies requirement for the fabrication of semiconductor devices. Thermal stability of the compound was investigated by thermogravimetric analysis (TGA). The TGA curve reveals that the decomposition temperature (T_d) at 5% weight loss is ca. 336 °C for S(TPA-bTV-CA), as shown in Fig. 1. The thermal stability of the material is good enough for the application in optoelectronic devices.

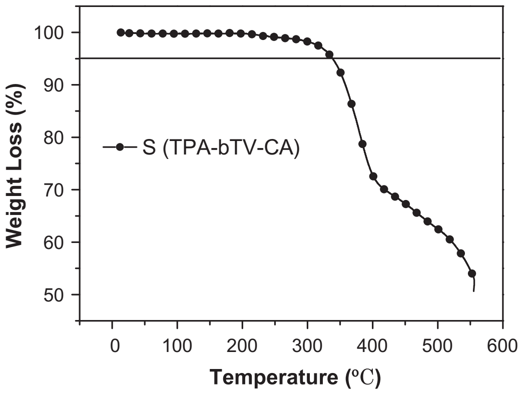

Fig. 1. TGA plot of S(TPA-bTV-CA).

3.2. Optical properties

The photophysical property of S(TPA-bTV-CA) was investigated by the measurement of UV–vis absorption spectra. Fig. 2 shows the absorption spectra of S(TPA-bTV-CA) solution with the concentration of 2.16×10^{-5} mol L^{-1} in chloroform and S(TPA-bTV-CA) film spin-coated on quarts plate. The solution absorption shows a broad absorption band covering the wavelength range from 300 to 650 nm, profiting from its D–A molecular structure connected with a conjugated pi-bridge. The optical absorption maxima (λ) were summarized in Table 1. S(TPA-bTV-CA) shows two distinct absorption bands. The first absorption band with absorption maxima (λ_s, max) at 402 nm for S(TPA-bTV-CA) can be identified with a delocalized excitonic π–π^* transition. The second one, the band peaking at 500–600 nm, is largely of the intramolecular charge transfer (ITC) transition between the TPA donor moiety and CA acceptor unit. The absorption coefficient of S(TPA-bTV-CA)) at its peak wavelength of 518 nm is 8.78×10^4 L mol^{-1} cm^{-1}, which indicates that the molecule exhibits strong absorbance in the visible region.

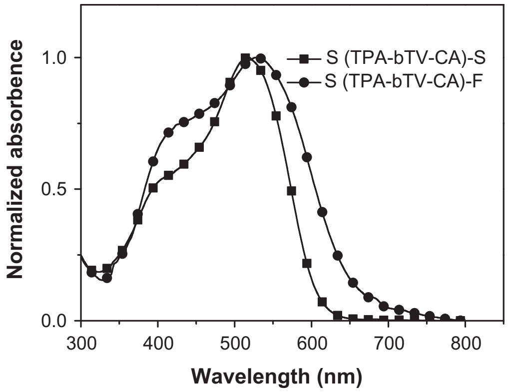

Fig. 2. UV–vis absorption spectra of S(TPA-bTV-CA) in chloroform solution and in film state.

Table 1
Absorption maxima (λ), absorption edge (λ_{edge}^{abs}), HOMO energy level, LUMO energy level and optical energy bandgap (E_g^{opt}) of S(TPA-bTV-CA).

Compound	$\lambda_{solution}$ (nm)	λ_{film} (nm)	λ_{edge}^{abs} (nm)	E_g^{opt} (eV)	HOMO[a] (eV)	LUMO[a] (eV)
S(TPA-bTV-CA)	402/518	430/533	720	1.72	−5.23	−3.51

[a] The electronic energy levels were calculated according to the following equations: HOMO = $-e$ (E_{onset}^{ox} + 4.4) (eV), and LUMO = E_g^{opt} + E_{HOMO}.

In comparison with absorption spectra of its dilute solution, the two absorption peaks of the film red-shifted by ca. 20 nm and broadened obviously, which indicates some aggregation of the molecule in the film. The absorption edge of S(TPA-bTV-CA) film is at ca. 720 nm, corresponding to the band gap of 1.72 eV.

3.3. Electrochemical properties and electronic energy levels

Electrochemical cyclic voltammetry was carried out for S(TPA-bTV-CA) film on Pt electrode, in order to estimate its HOMO and LUMO energy levels. Fig. 3 shows the cyclic voltammogram of S(TPA-bTV-CA) film. The HOMO energy level, the LUMO energy level, and the electrochemical bandgap (E_g^{opt}) of the small molecule were calculated from onset oxidation potentials (E_{onset}^{ox}) and onset reduction potentials (E_{onset}^{red}) according to the following equations [26]: $E_{HOMO} = -e$ (E_{onset}^{ox} + 4.4) (eV), and E_{LUMO} = -E_g^{opt} + E_{HOMO}, and the detailed results are listed in Table 1. Solution cyclic voltammetry (CV) measurements indicate that the highest occupied molecular orbital (HOMO) and the lowest unoccupied molecular orbital (LUMO) are −5.23 eV and −3.6 eV, respectively, corresponding to a band gap of 1.63 eV, in reasonable agreement with the optical band gap. Compared with the HOMO and LUMO energy levels (−5.87 eV and −3.91 eV respectively) of PC$_{70}$BM [27], the compound is suitable to be used as the photovoltaic donor blended with PC$_{70}$BM as acceptor in bulk-heterojunction OSCs.

3.4. Photovoltaic properties

Bulk-heterojunction OSCs were fabricated by using the molecule as donor, PC$_{60}$BM or PC$_{70}$BM as acceptor [28–30], with different donor/acceptor weight ratios and the general device structure is ITO/PEDOT: PSS/photoactive layer(70 nm)/Ca/Al.

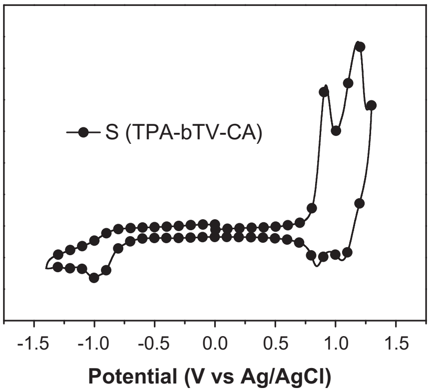

Fig. 3. Cyclic voltammograms of S(TPA-bTV-CA) films on Pt electrode in an acetonitrile solution of 0.1 mol/L Bu$_4$NPF$_6$ (Bu = butyl) with a scan rate of 100 mV/s.

Table 2
Photovoltaic properties of the OSCs based on the blend of S(TPA-bTV-CA):PC$_{60}$BM (or PC$_{70}$BM) with different weight ratios.

Active layer (weight ratio)	V_{oc} (V)	J_{sc} (mA/cm^2)	FF (%)	PCE (%)
S(TPA-bTV-CA):PC$_{60}$BM(1:1)	0.83	4.08	36	1.23
S(TPA-bTV-CA):PC$_{60}$BM(1:2)	0.80	4.36	38	1.34
S(TPA-bTV-CA):PC$_{60}$BM(1:3)	0.88	4.37	41	1.57
S(TPA-bTV-CA):PC$_{60}$BM(1:4)	0.69	2.83	33	0.64
S(TPA-bTV-CA):PC$_{70}$BM(1:3)	0.91	4.64	50	2.10

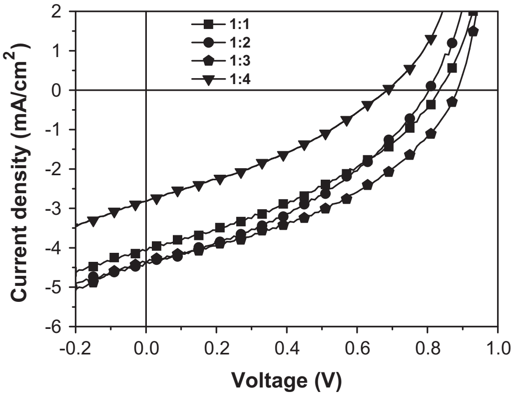

Fig. 4. Current density–voltage characteristics of the OSC devices based on the blends of S(TPA-bTV-CA)/PC$_{60}$BM (1:1, 1:2, 1:3, 1:4, w/w) with Ca/Al as the negative electrode under the illumination of AM 1.5, 100 mW/cm^2.

The optimized photovoltaic performance data of the OSCs, including the open circuit voltage (V_{oc}), short circuit current density (J_{sc}), fill factor (FF) and power conversion efficiency (PCE) values, are summarized in Table 2 for a clear comparison. Fig. 4 shows current density (J)–voltage (V) curves of the OSCs based on S(TPA-bTV-CA)/PC$_{60}$BM with different weight ratios of donor/acceptor in the active layer. It can be concluded that the donor/acceptor weight ratio is a key factor for a better performances of OSCs. For the devices with PC$_{60}$BM as acceptor, the device with a 1:1 blend weight ratio exhibits a J_{sc} of 4.08 mA/cm^2, a V_{oc} of 0.83 V, a FF of 36.3%, and a PCE of 1.23%. With increasing the donor/acceptor blend weight ratios from 1:1 to 1:4, the data of J_{sc}, FF and PCE, first increased and then decreased, but the V_{oc} does not display this tendency. The optimized device based on S(TPA-bTV-CA)/PC$_{60}$BM with blend weight ratio of 1:3 give the highest PCE of

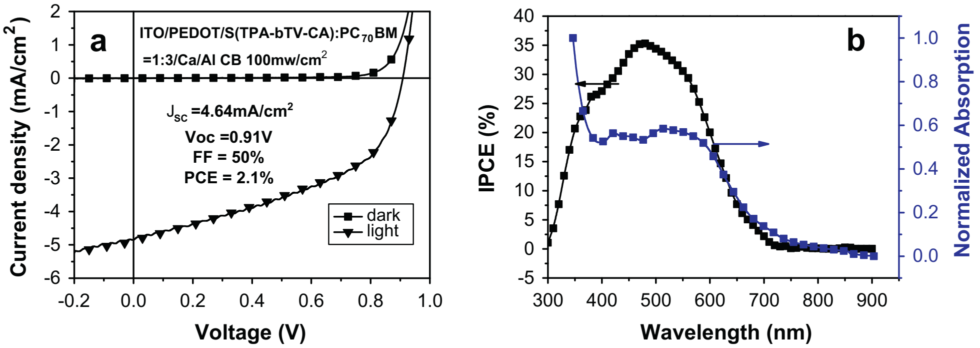

Fig. 5. (a) Current density–voltage characteristics of the OSC devices based on the blends of S(TPA-bTV-CA)/$PC_{70}BM$ (1:3, w/w) with Ca/Al as the negative electrode at dark and under the illumination of AM 1.5, 100 mW/cm^2; (b) IPCE spectrum of the OSC device.

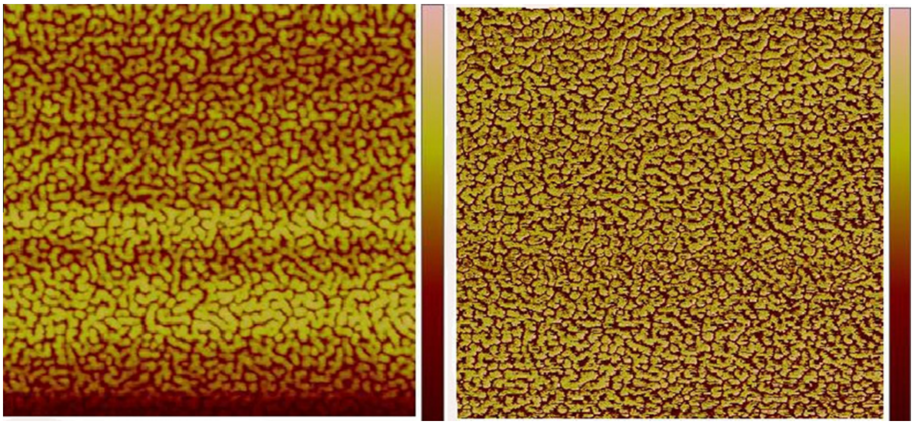

Fig. 6. AFM height (left) and phase (right) images of S(TPA-bTV-CA):$PC_{70}BM$ (1:3, w/w) blend (5 μm × 5 μm).

1.57%, with a J_{sc} of 4.37 mA/cm^2, a V_{oc} of 0.88 V and a FF of 40.9%. The decrease of J_{sc} to 2.83 mA/cm^2 for the ratio from 1:3 to 1:4 is maybe due to that the absorption of the active layer is reduced due to that the decrease of S(TPA-bTV-CA) content or the saturating in the active layer with PCBM leads to phase separation as reported in the literature [31]. In addition, the formation of the interpenetrating networks of the active layers needs proper weight ratio of donor and PCBM acceptor, which will lead to effective charge separation and charge transportation. Combined with a V_{oc} of 0.69 V and a FF of 32.7%, the device using the 1:4 ratio yields a PCE of 0.64%.

Fig. 5a shows the *J*–*V* curve of the OSC based on S(TPA-bTV-CA)/$PC_{70}BM$ (1:3, w/w), and for comparison, the photovoltaic data of the device were also listed in Table 2. Compared with the acceptor of $PC_{60}BM$ under the same device fabrication conditions, it is obvious that the device based on the acceptor of $PC_{70}BM$ delivered higher photovoltaic performance, and the PCE was improved from 1.57% with $PC_{60}BM$ as acceptor to 2.1% with $PC_{70}BM$ as acceptor. The better photovoltaic performance of $PC_{70}BM$ mainly benefits from its enhanced absorption in the visible region, specially 300–550 nm. In addition, the different acceptor of $PC_{60}BM$ and $PC_{70}BM$ could also have some influence on the active layer morphology.

As discussed above, the optimized device structure is ITO/PEDOT: PSS/photoactive layer (around 70 nm)/Ca/Al and with the weight ratio of S(TPA-bTV-CA):$PC_{70}BM$ = 1:3. The device exhibits good photovoltaic properties, and its V_{oc}, J_{sc}, FF, and PCE reached 0.91 V, 4.64 mA/cm^2, 50%, and 2.1%, respectively, under the illumination of AM 1.5, 100 mW/cm^2. Notably, the fill factor of 50% is one of the relatively high values reported for TPA derivatives or star-shaped donor-based OSCs with the probable reason of good film quality and relatively higher hole mobility of S(TPA-bTV-CA) which will be discussed in the following. The V_{oc} of 0.91 V is among the higher V_{oc} values of OSCs fabricated from organic star-shaped small molecules, which is consistent with the lower HOMO level (−5.23 eV) of S(TPA-bTV-CA).

Fig. 5b shows the input photon to converted current efficiency (IPCE) of the OSC based on S(TPA-bTV-CA)/$PC_{70}BM$ (1:3, w/w). The maximum quantum efficiency of the device reached ca. 35.5% at 480 nm. In addition, the wavelength range and the shape of the IPCE curves are coincident well with the absorption spectrum of the blend film,

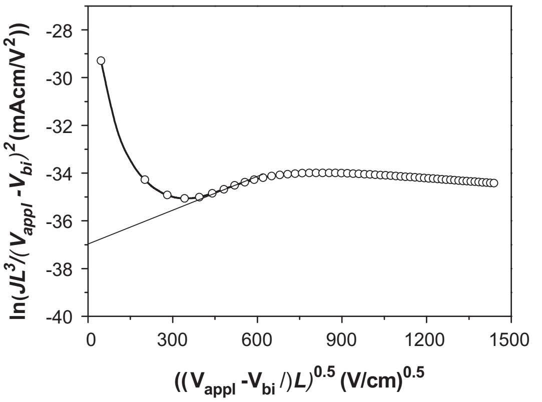

Fig. 7. Plot of ln(JL^3/V^2) versus $(V/L)^{0.5}$of the device ITO/PEDOT:PSS/S(TPA-bTV-CA)/Au for the measurement of hole mobility.

which indicates that the visible absorption of S(TPA-bTV-CA) did make a contribution to the photovoltaic conversion.

3.5. AFM morphology and hole mobility

Morphology of the photoactive layer plays a critical role in order to achieve good performance of OSCs. According to the literature [32], nanoscale phase separation enables a large interface area for exciton dissociation and a path for electron transport. The morphology of the S(TPA-bTV-CA):$PC_{70}BM$ (1:3, w/w) blend film was investigated by atomic force microscopy (AFM). Fig. 6 shows the AFM height and phase images of S(TPA-bTV-CA):$PC_{70}BM$ (1:3, w/w) blend film. The root-mean-square (rms) roughness of the film was 11.8 nm from the height image (see Fig. 6a). And the phase image in Fig. 6b shows visible phase separation with an elongated and ordered network of donor/acceptor domains, but the domain sizes are too big (larger than 100 nm). The relatively lower IPCE values and lower short circuit current density could be due to the big domain sizes.

Hole mobility of the molecule was measured by space-charge-limited-current (SCLC) method [33] with the device structure of ITO/PEDOT:PSS/S(TPA-bTV-CA) film/Au (Fig. 7), and the thickness of S(TPA-bTV-CA) film is 94 nm. Fig. 7 shows the plot of ln(JL^3/V^2) versus $(V/L)^{0.5}$of the device, and the hole mobility of S(TPA-bTV-CA) calculated from the results is $2.03 \times 10^{-4}\ \mathrm{cm^2\ V^{-1}\ s^{-1}}$, indicating that S(TPA-bTV-CA) possesses a relatively higher hole mobility in comparison with other TPA-based molecules.

4. Conclusions

A new star-shaped D–π–A molecule S(TPA-bTV-CA) with triphenylamine (TPA) as core and donor unit, CA as end group and acceptor unit, and 2,2′-bithiophene-vinylene (bTV) as π−bridge, was designed and synthesized for the application as donor material in solution-processed bulk-heterojunction organic solar cells (OSCs). S(TPA-bTV-CA) shows good solution processability and thermal stability, strong absorption, deep HOMO energy level and relatively higher hole mobility. The PCE of the bulk heterojunction OSC based on a blend of S(TPA-bTV-CA) and PC_{70}-BM (1:3, w/w) reached 2.1% with a J_{sc} of 4.64 mA/cm^2, a V_{oc} of 0.91 V and a FF of 50%, under the illumination of AM.1.5, 100 mW/cm^2.

References

[1] Y.F. Li, Acc. Chem. Res. 45 (2012) 723–733.
[2] S. Roquet, A. Cravino, P. Leriche, O. Aleveque, P. Frere, J. Roncali, J. Am. Chem. Soc. 128 (2006) 3459–3466.
[3] S. Karpe, A. Cravino, P. Frere, M. Allain, G. Mabon, J. Roncali, Adv. Funct. Mater. 17 (2007) 1163–1171.
[4] J. Roncali, P. Leriche, A. Cravino, Adv. Mater. 19 (2007) 2045–2060.
[5] D. Demeter, T. Rousseau, P. Leriche, T. Cauchy, R. Po, J. Roncali, Adv. Funct. Mater. 21 (2011) 4379–4387.
[6] E. Ripaud, T. Rousseau, P. Leriche, J. Roncali, Adv. Energy Mater. 1 (2011) 540–545.
[7] C.-Q. Ma, E. Mena-Osteritz, T. Debaerdemaeker, M.M. Wienk, R.N.J. Janssen, P. Bauerle, Angew. Chem. Int. Ed. 46 (2007) 1679–1683.
[8] C.-Q. Ma, M. Fonrodona, M.C. Schikora, M.M. Wienk, R.A.J. Janssen, P. Bauerle, Adv. Funct. Mater. 18 (2008) 3323–3331.
[9] Y.S. Liu, X.J. Wan, B. Yin, J.Y. Zhou, G.K. Long, S.G. Yin, Y.S. Chen, J. Mater. Chem. 20 (2010) 2464–2468.
[10] X. Sun, Y. Zhou, W. Wu, Y. Liu, W. Tian, G. Yu, W. Qiu, S. Chen, D. Zhu, J. Phys. Chem. B 110 (2006) 7702–7707.
[11] L.L. Xue, J.T. He, X. Gu, Z.F. Yang, B. Xu, W.J. Tian, J. Phys. Chem. C 113 (2009) 2911–12917.
[12] A.B. Tamayo, B. Walker, T.Q. Nguyen, J. Phys. Chem. C 112 (2008) 11545–11551.
[13] C. He, Q.G. He, Y.P. Yi, G.L. Wu, F.L. Bai, Z.G. Shuai, Y.F. Li, J. Mater. Chem. 18 (2008) 4085–4090.
[14] J. Zhang, Y. Yang, C. He, Y.J. He, G.J. Zhao, Y.F. Li, Macromolecules 42 (2009) 7619–7622.
[15] D. Deng, Y. Yang, J. Zhang, C. He, M.J. Zhang, Z.G. Zhang, Z.J. Zhang, Y.F. Li, Org. Electron. 12 (2011) 614–622.
[16] D. Deng, S.L. Shen, J. Zhang, C. He, Z.J. Zhang, Y.F. Li, Org. Electron. 13 (2012) 2546–2552.
[17] (a) J. Zhang, D. Den, C. He, M.J. Zhang, Z.G. Zhang, Z.J. Zhang, Y.F. Li, Chem. Mater. 23 (2010) 817–822;
(b) P. Arsenyan, E. Paegle, S. Belyakov, Tetrahedron Lett. 51 (2010) 205–208.
[18] (a) P.F. Xia, X.J. Feng, J.P. Lu, S.W. Tsang, R. Movileanu, Y. Tao, M.S. Wong, Adv. Mater. 20 (2008) 4810–4815;
(b) M.C. Cui, Z.J. Li, R.K. Tang, H.M. Jia, B.L. Liu, Eur. J. Med. Chem. 46 (2011) 2908–2916.
[19] Y.M. Sun, G.C. Welch, W.L. Leong, C.J. Takacs, G.C. Bazan, A.J. Heeger, Nature Mater. 11 (2012) 44–48.
[20] G. Yu, J. Gao, J. Hummelen, F. Wudl, A.J. Heeger, Science 270 (1995) 1789–1791.
[21] Y. Lin, Z.-G. Zhang, H. Bai, Y. Li, X. Zhan, Chem. Commun. 48 (2012) 9655–9657.
[22] Y. Lin, P. Cheng, Y. Li, X. Zhan, Chem. Commun. 48 (2012) 4773–4775.
[23] Y. Liu, X. Wan, F. Wang, J. Zhou, G. Long, J. Tian, J. You, Y. Yang, Y. Chen, Adv. Energy Mater. 1 (2011) 771–775.
[24] J. Zhou, X. Wan, Y. Liu, Y. Zuo, Z. Li, G. He, G. Long, W. Ni, C. Li, X. Su, Y. Chen, J. Am. Chem. Soc. 134 (2012) 16345–16351.
[25] Z.C. He, C.M. Zhong, S.J. Su, M. Xu, H.B. Wu, Y. Cao, 10.1038/nphoton.2012.190.
[26] Q.J. Sun, H.Q. Wang, C.H. Yang, Y.F. Li, J. Mater. Chem. 13 (2003) 800.
[27] Y.J. He, G.J. Zhao, B. Peng, Y.F. Li, Adv. Funct. Mater. 20 (2010) 3383–3389.
[28] M.M. Wienk, J.M. Kroon, W.J.H. Verhees, J. Knol, J.C. Hummelen, P.A. van Hal, R.A.J. Janssen, Angew. Chem. Int. Ed. 42 (2003) 3371.
[29] F.B. Kooistra, V.D. Mihailetchi, L.M. Popescu, D. Kronholm, P.W.M. Blom, J.C. Hummelen, Chem. Mater. 18 (2006) 3068.
[30] B.C. Thompson, J.M.J. Frechet, Angew. Chem. Int. Ed. 47 (2008) 58.
[31] Wenseleers, F. Stellacci, T. Meyer-Friedrichsen, T. Mangel, C.A. Bauer, S.J.K. Pond, S.R. Marder, J.W. Perry, J. Phys. Chem. B. 106 (2002) 6853.
[32] G. Li, V. Shrotriya, J.S. Huang, Y. Yao, T. Moriarty, K. Emery, Y. Yang, Nature Mater. 4 (2005) 864–868.
[33] Q. Zheng, B.J. Jung, J. Sun, H.E. Katz, J. Am. Chem. Soc. 132 (2010) 5394–5404.